ICAS PAPER No. 72-39

THEORETICAL AND EXPERIMENTAL INVESTIGATIONS
ON THE PROBLEM OF AERODYNAMIC HEATING
OF RE-ENTRY VEHICLES

by
J. P. Hoffmann, Senior Group Engineer, and
A. Bäuerle, Senior Engineer
ERNO Raumfahrttechnik, GmbH
Bremen, Germany

The Eighth Congress of the International Council of the Aeronautical Sciences

INTERNATIONAAL CONGRESCENTRUM RAI-AMSTERDAM, THE NETHERLANDS
AUGUST 28 TO SEPTEMBER 2, 1972

Price: 3. Dfl.

THEORETICAL AND EXPERIMENTAL INVESTIGATIONS ON THE PROBLEM OF AERODYNAMIC HEATING OF RE-ENTRY VEHICLES

J. P. Hoffmann, H. J. Leue, A. Bäuerle

ERNO RAUMFAHRTTECHNIK GMBH
28 Bremen, W-GERMANY

Abstract

Surface oil flow and Schlieren photographs, centreline pressure distributions as well as heating distributions on models of the ERNO lifting body configuration LB-21 are presented and analyzed. The best data were obtained in three hypersonic facilities at M_∞ between 8 and 20 and $Re_\infty/_{ft}$ from $5 \cdot 10^4$ to $9 \cdot 10^5$. The accuracy of heat transfer predictions by means of simplifying strip flow and axisymmetric assumptions are discussed. The influence of crossflow corrections accounting for three dimensionality is shown. Radiation equilibrium surface temperatures for maximum heating rates observed in the test program are given.

Nomenclature

a	speed of sound, exponent
c	specific heat of model skin
cp	pressure coefficient
D	diameter of equivalent disk, local body
F	diffusion function after ref. 8 (width
h	heat transfer coefficient based on enthalpy
h_2	metric coeff.f.curvilinear coord. system
i	enthalpy
j	exponent
L	reference length
$\mathcal{L}$	Lewis number function after ref. 12
Le	Lewis number
M	Mach number
p	pressure
Pr	Prandtl number
$\dot{q}$	heating rate
R	leading edge radius
Re	Reynolds number
s	surface length in crossflow direction
t	dimensionless static enthalpy $= i/i_E$,
i_E	$2{,}119 \cdot 10^8$ (ft^2/s^2)
T	temperature
u	crossflow velocity
V	axial velocity
V_N	normal component of velocity
x	streamwise surface coordinate
$\bar{x}$	distance along streamline
xeq	equivalent distance
y	crosswise surface coordinate
α	angle of attack
β	yaw angle, velocity grad.param., eq. 4
Γ	heat transfer function - eq. 3
δ	wall thickness of thin skin model
ϵ	emissivity
ϑ	stagnation enthalpy ration I/Ie
Θ	angle measured for stagnation point
λ	sweep angle of lead.edge,heat cond.coeff.
μ	absolute viscosity
ξ	Shock standoff angle
ϱ	density
τ	incremental time

Subscripts

∞	freestream condition
o,s	stagnation condition
aw	adiabatic wall
ℓ	centreline
e	edge of boundary layer
e_{ff}	effective value
r	reference condition
ℓ	stagnation line
w	wall condition

Introduction

ERNO Raumfahrttechnik had been permanently engaged in the problems of atmospheric reentry for a number of years. Investigations in aerodynamics, flight control, aerothermodynamics and thermal control have been conducted in conjunction with configuration developments. Experience shows that theoretical studies and wind tunnel testing does not suffice for a thorough expertise in reentry technology. This leds to the proposal for an experimental free-flight vehicle which may be launched by the EUROPE I launcher and reenters the atmosphere from a 200 km - orbit. Preliminary investigations which are discussed in ref. 1 resulted in a lifting body configuration shown in fig.1.

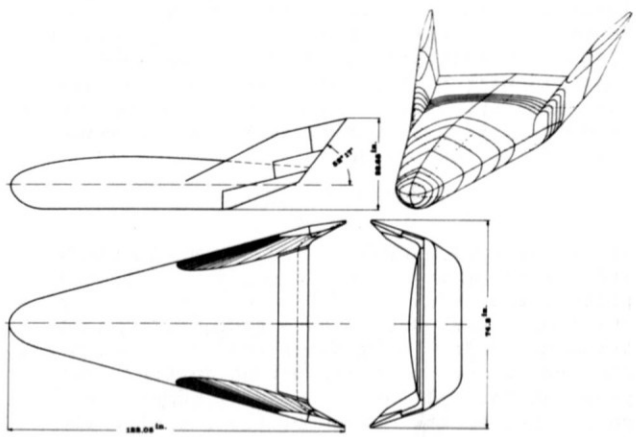

MAIN DIMENSIONS OF LB-21

Fig. 1

The vehicle with a gross-weight of approx. 1500 lbs ($W/S = 100$ kp/m^2) attains max. lift to drag ratios of 4.5 in the subsonic region and 1.3 in hypersonic flight. This paper will focus attention on recent results of hypersonic heat transfer experiments with different small-scale models of the proposed configuration. The investigations have been conducted under contract of the Federal Ministry of Education

and Science (BMBW-GFW) in close cooperation with the DFVLR and the Technical University at Aachen. Special emphasise was given on the angle of attack variation at the max. heating flight regime. Comparisons with theory were made in order to define the appropriate methodology for computing flight heating rates in further trajectory shaping and material investigations.

Analytical Techniques

Under the aspect of minimization of the total heat input a high angle of attack flight is desirable due to the reduced reentry time. This implies a considerably complication since the flow field is significantly modified by threedimensional effects. Furthermore the pressure gradients imposed on the boundary layer by the inviscid flow are not in the direction of the outer flow which causes transverse components of motion within the surface flow as has been clarified by several authors.[2,3] A simplification yield the decoupling of the three-dimensional boundary layer as in the case of incompressible flow. Approximatly the independence principle might be used by neglecting higher order terms in the crossflow velocity and the lateral derivatives with respect to a streamline coordinate system.[4,5,6] The methods of incompressible boundary layers remain applicable at high Mach number flows if compressibility correlations[7] are used. However the application of small crossflow theories requires the detailed knowledge of the inviscid three-dimensional flow field which could not be treated analytically for the proposed configuration. Therefore simplifying assumptions are necessary to describe the boundary layer edge conditions. The modified Newtonian theory was used for pressure calculations on the spherical nose as well as on the yawed leading edges. For the bottom centerline the Newtonian pressure after an expansion from the stagnation point to the surface angle was compared with predictions obtained on a pointed cone with the semiapex angle taken as the angle of attack and in addition with the following value for a sharp wedge:

$$C_p = \frac{2(\sin\alpha)\cdot\sin(\alpha+\delta)}{\cos(\delta)} \qquad (1)$$

The difference δ between the angle of attack and the shock angle was taken from Schlieren photographs (fig. 7 and 8). Corresponding to the flow field estimations, simplifying heat transfer prediction methods had to be employed. The heat transfer distributions on the blunt prow and the cylindrical leading edges were calculated by the method of local similarity developed by N.B. Cohen and I.E. Beckwith.[8,9] This was accomplished in applying the following set of equations:[8]

$$\frac{\dot{q}_w}{\dot{q}_{w,s}} = \left(\frac{\left(\frac{\rho_w \mu_w}{\beta \cdot te} \cdot du_e/dx\right)}{\left(\frac{\rho_w \mu_w}{\beta \cdot te} \cdot du_e/dx\right)_s} \right)^{1/2} \cdot \Gamma \qquad (2)$$

Where the heat transfer function GAMMA is defined as

$$\Gamma = \frac{\left(\frac{1+F_w}{Pr_w} \cdot f_w'\right) \cdot}{\left(\frac{1+F_w}{Pr_w} \cdot f_w'\right)_s} \qquad (3)$$

and the velocity gradient parameter:

$$\beta = \frac{2\cdot t_s \cdot du_e/dx}{\rho_w \mu_w \cdot u_e^2 \cdot te \cdot (R/L)^{2j} \cdot \Gamma^2} \int_0^x \rho_w \mu_w \cdot u_e \left(\frac{R}{L}\right)^{2j} \Gamma^2 \, dx \qquad (4)$$

(j=0 Yawed infinite Cylinder, j=1 Sphere)
The prime at f_w' of eq. 3 denotes the differentiation of the wall enthalpy ratio with respect to the normal similiarity coordinate η . As can be seen an iterative procedure is required because of the interdependency between β and $(f_w'/f_{w,o}')$. A simplification was obtained by the use of the correlation equation for $(f_w'/f_{w,o}')$ given in ref. 8. This method was also applied for the estimation of the spanwise heat transfer distribution on the windward side at angle of attack. The crossflow calculations were started at the windward centerline with a crossflow velocity-gradient analogous to that on a circular disk normal to the freestream velocity vector. This gradient is given by a correlation proposed from M.H. Bertram and A. Henderson:[10]

$$\left(\frac{\partial u_e}{\partial y}\right)_{\mathcal{L}} = (0.745 + 3.14 \cdot \frac{R}{D}) \cdot \frac{a_{o,N}}{D} \qquad (5)$$

The term $a_{O,N}$ is the stagnation sonic velocity for the freestream normal component $V_{N,\infty} = V_\infty \cdot \sin\alpha$; R is the edge radius and D is the diameter of the equivalent disk or the local body width. Since this gradient implies a relationship to the stagnation point velocity gradient on a sphere the absolute heating rate on the centerline was obtained from the similiarity solution for the axisymmetric stagnation point. A rude estimation of the spanwise pressure distribution consisting of a slight decay from the theoretical centerline value to a infinite cylinder stagnation pressure on the leading edge shoulder followed by a Newtonian expansion over the leading edge had to be applied because of a lack of experimental data. As discussed later this estimation does not fit the measured heating distributions in all sections. An improvement might be expected from supplemental pressure measurements. The absolute local heat transfer on the blunted outer edges and the slab portion was finally obtained by relating the resulting distributions on the appropriate stagnation values given by the correlation equations[8] (6) and (7) for the sphere and the infinite yawed cylinder respectively.

$$\dot{q}_{w,o} = 0.767 \cdot (\rho_e \mu_e)_o^{0.43} \cdot (\rho_w \mu_w)_o^{0.07} \cdot Pr_{w,o}^{-0.67} \cdot (du_e/dx)_o^{0.5} \cdot (i_{AW} - i_W) \qquad (6)$$

$$\dot{q}_{w,\mathcal{L}} = 0.57 \cdot (\rho_e \mu_e)_{\mathcal{L}}^{a} \cdot (\rho_w \mu_w)_{\mathcal{L}}^{(0.5-a)} \cdot Pr_{w,\mathcal{L}}^{-0.67} \cdot (du_e/dx)_{\mathcal{L}}^{0.5} \cdot (i_{AW} - i_W) \qquad (7)$$

Where the exponent "a" is taken as 0,45 for $\frac{\rho_e \cdot \mu_e}{\rho_w \cdot \mu_w} \leq 1$ and 0,67 for density-viscosity product ratios greater than 1. For reasons of

comparison results from the laminar $\rho_\tau \mu_\tau$ method originally developed by R.A. Hanks have been included. As is shown in ref.11 the application of the streamwise momentum integral equation in connection with the Reynolds analogy and the definition of an equivalent length coordinate leads to the following laminar flat plate analogy for the heat transfer coefficient:

$$h = 0.332 \cdot \mathcal{L} \frac{}{Pr_\tau^{0.645}} \left(\frac{\rho_\tau \mu_\tau \cdot u_e}{Xeq_{,LAM}} \right)^{0.5} \qquad (8)$$

$\mathcal{L}$ denotes the diffusion function after Fay and Riddell[12] which becomes 1 with Le = 1. Equation 8 is generally applicable in laminar flows provided the pressure gradient and flow history effects on the streamline are accounted for by a proper definition of $\rho_\tau \mu_\tau$ and $Xeq_{,LAM}$. This implies the opportunity of treating three-dimensional boundary layers by taking into account streamline divergence effects. In the present application this was accomplished by calculating $Xeq_{,LAM}$ on the windward centerline by means of the Vaglio-Laurin[5] expression for streamline curvature:

$$\frac{1}{h_2} \frac{\partial h_2}{\partial \bar{x}} = \frac{1}{V_e} \cdot \frac{\partial u_e}{\partial s} \qquad (9)$$

The equivalent distance was then obtained from:

$$Xeq_{,LAM.} = \frac{\int_0^x h_2^2 \, dx}{h_2^2} \qquad (10)$$

The crossflow-velocity gradient was again taken from eq. 5 but by assuming a sharp leading edge in order to obtain a direct solution for $Xeq_{,LAM}$. The reference value of the density-viscosity product $\rho_\tau \mu_\tau$ was replaced by the boundary layer edge value $\rho_e \mu_e$ for strip calculations. For stagnation line heating predictions eq. 8 has been used in connection with the $Xeq_{,LAM}$ and $\rho_\tau \mu_\tau$ correlations given in ref. 11. These equations were developed from similiarity solutions discussed before.

Facilities and Test Conditions

Several hypersonic facilities have been engaged during the course of this program in order to extend the prediction on a wider range of the reentry trajectory and to provide the possibility of data comparison.

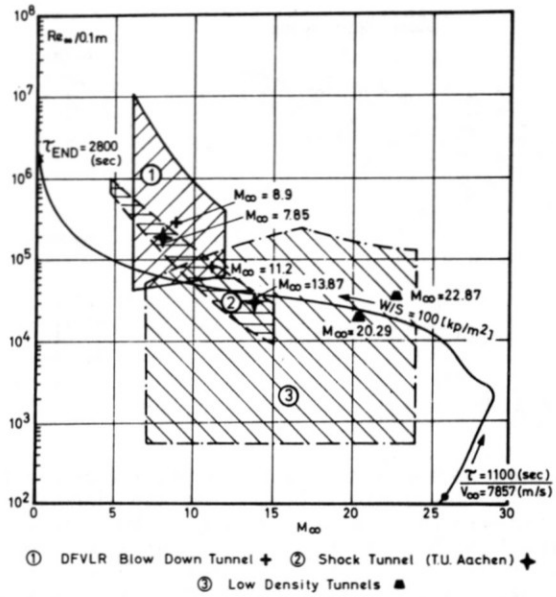

MACH - REYNOLDS - DOMAIN OF APPLIED HYPERSONIC FACILITIES

Fig. 2

The discussed test data were obtained in the 20 in. Shock tunnel of the Techn. University at Aachen[13], in the 20 in. and 6 in. hypersonic Blow Down tunnels of DFVLR at Porz/Wahn[14] and in the 10 in. -Low Density tunnel of DFVLR - AVA Göttingen[15]. The test conditions are shown in fig. 2 and may be seen in detail from table1. A pneumatic injection technique was applied in both latter, long operating tunnels providing on insertion time toward the center of the order of 0.1 seconds.

Test Methods and Data Reduction

Various measurements techniques have been applied due to different operating time and maximum model scale available in the facilities.

TABLE 1 - SCHEDULE OF EXPERIMENTAL INVESTIGATIONS

SERIES Nº	FACILITY	TEST-MEDIUM	MEASUREMENT CONDITIONS				SCOPE OF MEASUREMENTS			MODEL SPECIFICATION	
			M_∞	Re_∞/ft	P_{STAG}(at)	T_{STAG}(K)	$\alpha°$	$\eta°$	MEAS. TECHNIQUE	MATERIAL	SCALE
1	SHOCK TUNNEL of TECHN. UNIV. AACHEN (ϕ = 20 INCH)	H_2/N_2	7.85	6.1×10^5	0.31	2448	0,10,15 17,45	0,10	16 PLATIN RESIST. THERMOMETERS	STAINLESS STEEL	0.10
2			13.87	8.8×10^4	0.02	2336	45	0	7 PIEZO PRESSURE GAGES SCHLIEREN - PHOTOGR.		
3	BLOW DOWN TUNNEL OF DFVLR - PORZ - WAHN (ϕ = 20 INCH)	AIR	11.2	2.3×10^5	22	1023	0,10,15 20,30,40	0,5,10	THERMOCOLOR PAINTING	SILICON RUBBER	0.10
4	(ϕ = 6 INCH)		8.9	9×10^5	25	880	0,15,30	0,5,10	TEMPILAQ SPRAY OIL-FLOW & SCHLIEREN - PHOTOGR.	STYCAST - 2651 COMPOUND	0.03
5	LOW DENSITY TUNNEL of DFVLR - AVA GOETTINGEN (ϕ = 10 INCH)	N_2	20-23	4.8×10^4 to 1.1×10^5	30-100	1400-1600	0-35	0	9 Ni-Cr-Ni - THERMO-COUPLES	0.08 INCH thin skin nickel-model	0.03

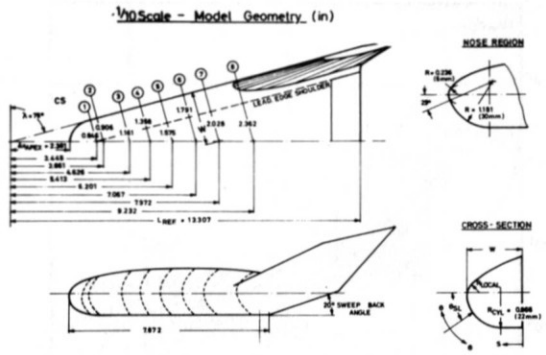

Fig. 3

Two model scales were employed. A 1/10 scale as shown in Fig. 3 was utilized for the shocktunnel testing and the thermal mapping tests in the 20 in. Blow Down tunnel whereas the models for 6 in. resp. 10 in. channels at Porz/Wahn and Göttingen were scaled to 3/100.The Shock tunnel measurement on the windward and leeward side have been obtained from separat runs where the sting was mounted on the side opposite to the instrumented surface in order to avoid sting effects. Heat transfer and pressure measurements as well as Schlieren photographs have been carried out. The sixteen thin film heat transfer and seven piezo pressure gages on each side were located along the centreline and in sections normal to the leading edge.

The data were then reducted from oscillographs by the well known methods by R.J. Vidal[16] and others. The effective measurement time was of the order of 2 milliseconds. Additional heat transfer data were obtained from thermal mapping tests. A four color-change paint has been used on 0,10-scale molded silicon rubber model and three different rated Tempilaq coatings on the smaller Stycast - model. Average thermal properties of $\sqrt{\lambda \varrho c} = 0.0147 \left(\frac{cal}{cm^2\, s^{1/2} K}\right)$ for silicon rubber and 0.0246 for Stycast respectively have been assumed. Motion picture photography with a framing rate of 34 frames per second was utilized in recording the progression of the isotherms over the model, 16 mm - color film for the Thermocolor tests and black- and - white film for the Tempilaq measurements have been used. The first step in data reduction procedure was the tracing of isotherms by projection the films on enlarged photographs of a grid model taken at the appropriate positions.

The heat transfer coefficient may then be determined from the solution if the governing transient one-dimensional heat conduction equation given in ref. 17.

A detailed analysis regarding the accuracy in applying this equation on thermal mapping tests has been given by several authors.[18,19] Nevertheless, a simplified reduction technique provide comparative measurements on spheres constructed of the material under consideration. The time-dependent progression of the isotherms may than be related to heat transfer calculations providing calibration curves due to each color or phase charge history. Fig. 4 shows experimental data obtained from Schepers and Will[20] on spheres of different radii where THERMOCOLOR and TEMPILAQ coatings have been applied.

The theory of local similiarity (eq. 2 through 6) has been used in calibrating these results. Thermocouples installed in the stagnation region of the models indicated the initial temperature rise which is of particular interest. The time between two runs has been taken care to be long enough for the reproduction of isothermal conditions on the model. In addition to the heat transfer measurements Schlieren and oil flow pattern photographs have been taken from the Stycast model.[20] In the Low Density tunnel of AVA Göttingen the transient thin skin technique has been used for local heat transfer measurements. The 0.03 scale nickel model was fabricated by an electroforming technique. For the temperature measurements Nickel-Chromium wires of about 0,04 in. diameter were soldered into the 0,08 in. wall forming in this connection Ni-Cr-Ni-thermocouples. The transient temperatures were then recorded on an U-V-oscillograph and simultaneously differentiated with respect to the time. The local heat transfer was calculated from the following heat balance equation

$$\dot{q}_w = \varrho_w \cdot c_w \cdot \delta \left(\partial T_w / \partial \tau\right)_{\tau_{MIN} < \tau < \tau_{MAX}} \qquad (11)$$

where δ, ϱ_w, c_w denote the wall thickness and density respect. specific heat of the model material.

Nine thermocouples were located along the centreline and on three stations at the leading edge. The measurement time did not exceed 1 second in order to avoid significant lateral heat conduction.Before each run the model was exposed to a cool airstream to provide isotherm. conditions.

Construction of Calibration Curves for Thermal Mapping Tests

(1) EXPERIMENTALLY DETERMINED COLOR AND PHASE CHANGE HISTORY

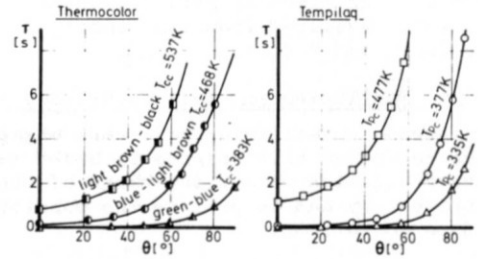

(2) HEAT TRANSFER DISTRIBUTION ON CALIBRATION SPHERE'S (R_N = 17.5 and 30.0mm)

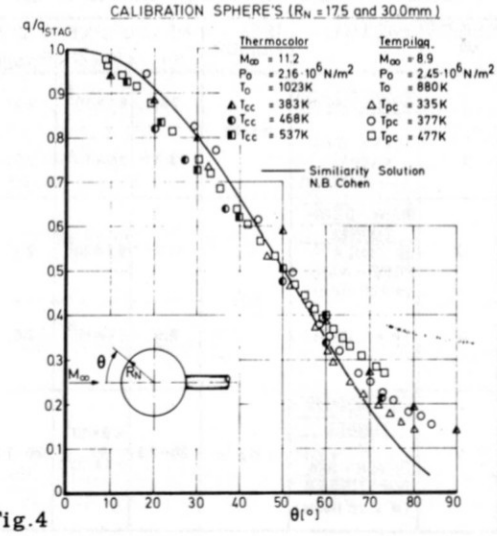

Fig. 4

Results and discussion

Only windward surface data are discussed in the following since the fuselage bottom is exposed to the most critical pressure and thermal loads at high angle of attack flight. The data are compared with laminar heat transfer calculations because no indication of transition was observed. Of considerably interest with respect to a proper interpretation of heat transfer and pressure distributions are surface flow studies.

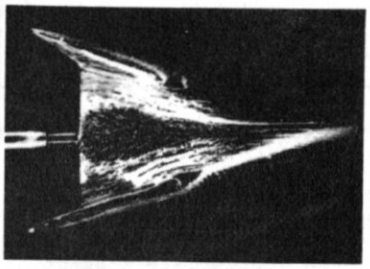

OIL-FLOW PATTERN OF LB-21

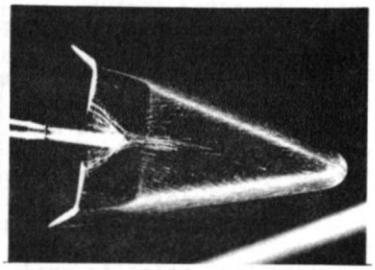

$M_\infty = 8.9$
$Re_\infty/ft = 9 \cdot 10^5$
$p_0 = 2.45 \cdot 10^6 [N/m^2]$
$T_0 = 880°K$
$\alpha = 15°, \Phi = 0°$

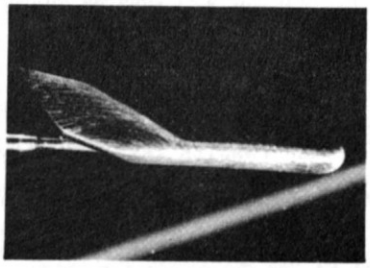

Fig.5

Figures 5 and 6 show photographs of oil flow patterns taken from the LB-21 Stycast model after runs with 15° and 30° angle of attack. Along the blunt leading edges the expected crossflow patterns for swept cylinders may be seen. The streamline rise provides a decrease of nose influence on the leading edge at $\alpha = 30°$. The stagnation line appears located on the cylindrical portion in both cases but has shifted considerably toward the leading edge shoulder for 30° inclination. The streamlines on the flat bottom show an inflow toward the fuselage centreline at 15° but become almost straight at 30° angle of attack. This phenomenon would be changed substantial at higher angles of attack when crosswise gradients start to turn the flow out of the centre. On the upper surface nose bluntness effects may be detected at both angles of attack. A centre region of increased pressure may be defined where the flow is processed through the bowed shock in front of the spherical nose. The dissipation of the prow effect provides an outflow from the leeward centreline. At 30° angle of attack flow separation seems to appear shortly above the juncture to the cylindrical leading edge. Supplemental Schlieren photographs have been taken at Mach 8.9 in the Blow Down tunnel and at Mach 7,85 in the Shock tunnel. The figures (7) and (8) show side photogr. taken in both tunnels at various angles of attack. Only the freestream conditions for the Shock tunnel runs belonging to the pictures on the right are noted in the figures.

The heat transfer analysis may be started on the centreline. Fig. 9 shows pressure distributions on the plane of symmetry which were obtained in the Shock tunnel at Mach 7,85 and 13,87. The data are related to the stagnation pressure after a normal shock and have been plotted over a surface coordinate starting at the actual stagnation point on the sphere due to the angle of attack. This surface coordinate was normalized by the total model length in planview measured from the theorectical apex to the trailing edge (fig. 3). Analytical values for the windward side were obtained from the modified Newtonian theory as well as from sharp cone and wedge calculations with the semiapex angle taken as the angle of attack of the fuselage. At zero inclination the data lie consistently above the value for zero pressure coefficient. This is caused by nose bluntness and viscous interaction effects in the forward portion and by induced pressure due to leading edge bluntness in a larger distant from the blunt prow. The bluntness effects on the centreline rapidly diminish while increasing the angle of attack resulting in a constant pressure at $\alpha = 45°$.

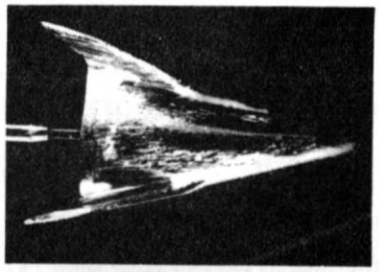

OIL-FLOW PATTERN OF LB-21

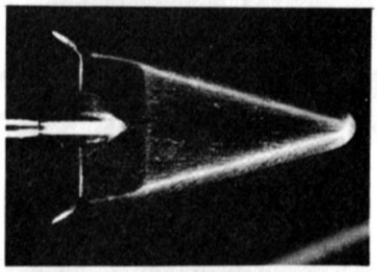

$M_\infty = 8.9$
$Re_\infty/ft = 9 \cdot 10^5$
$p_0 = 2.45 \cdot 10^6 [N/m^2]$
$T_0 = 880°K$
$\alpha = 30°, \Phi = 0°$

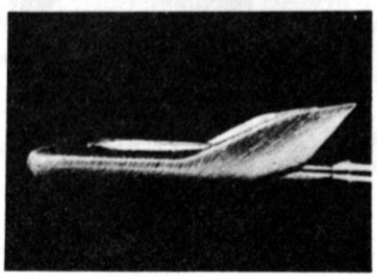

Fig. 6

SCHLIEREN PHOTOGRAPHS OF LB-21

$M_\infty = 7.85$ $Re_\infty/ft. = 6.1 \cdot 10^5$

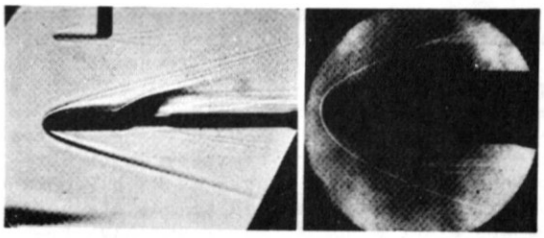

$\alpha = 0°$ $\Omega = 0°$

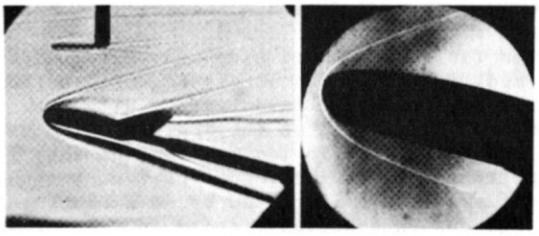

$\alpha = 15°$ $\Omega = 0°$

Fig. 7

SCHLIEREN PHOTOGRAPHS OF LB-21

$M_\infty = 7.85$ $Re_\infty/ft. = 6.1 \cdot 10^5$

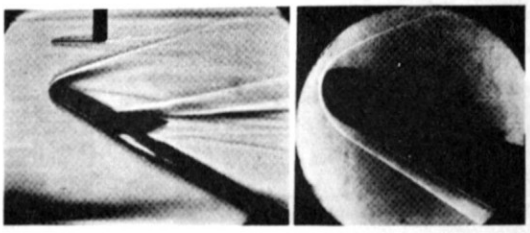

$\alpha = 30°$ $\Omega = 0°$

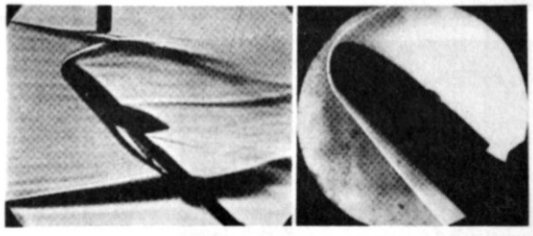

$\alpha = 45°$ $\Omega = 0°$

Fig. 8

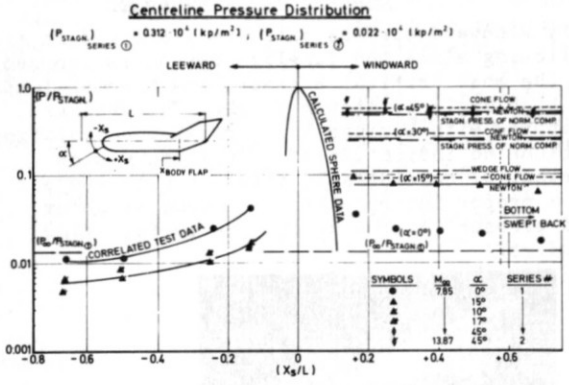

Fig. 9

Fig. 10 shows the corresponding heat transfer distributions where the data have been normalized by means of the appropriate stagnation point value*. It should be noted that the surface coordinate is now measured from the nose tip in order to show the stagnation point shift. The laminar $\rho_\infty \mu_\infty$ flat plat method (eq. 8) has been applied with respect to different pressure assumptions as indicated in the figure. At angles of attack 15° to 45° the strip theory was modified by the sharp delta wing crossflow correction to account for streamline divergence. In addition the modified similiarity solution using Bertram & Hendersons[10] circular disk correlation for the crossflow velocity gradient is shown. A parallel shock front at the bottom was assumed for 15° and 30° angle of attack whereas the wedge pressure from eq. 1 was applied at $\alpha = 45°$.
The similiarity solution in this acaption seems to overpredict the centreline heating at 15° and 30°. At $\alpha = 45°$ the results fall slightly below the shock tunnel data.
Fig. 11 represents a comparison of theoretical two-dimensional calculations with test results on the blunt leading edge. The location of the stagnation line has been determined from the infinite cylinder equation:

$$\tan \Theta_{\ell} = \frac{\sin \alpha}{\cos\alpha \cdot \cos \lambda + \tan \beta \cdot \sin \lambda} \qquad (12)$$

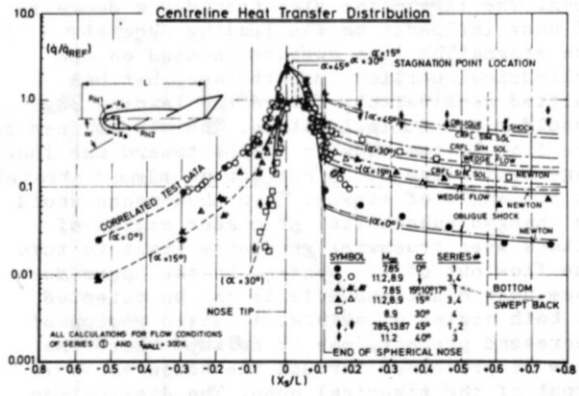

Fig. 10

*. $q_{REF.,R=0.03m}\left(\frac{cal}{cm^2\,s}\right)$ SERIES ① ② ③ ④ = 21.39 / 5.66 / 1.77 / 2.70

Heat Transfer Distribution Along the Leading Edge

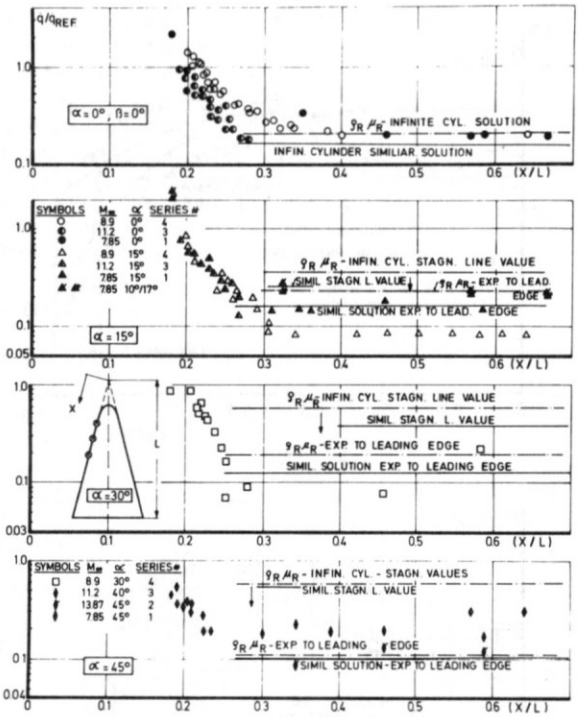

Fig. 11

Circumferential Heating Distribution Around Backward Body Sections

α = 0°, β = 0°

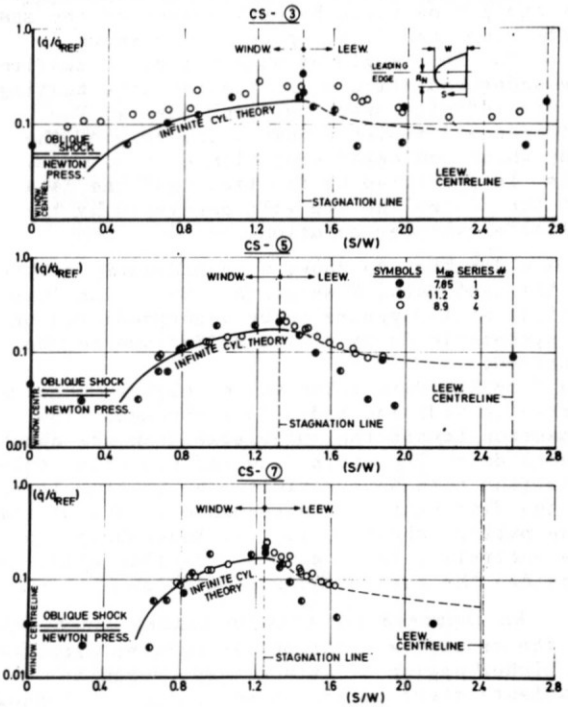

Fig. 12

The value on the leading edge was then obtained from the local similiarity solution extended to the theoretical expansion angle. The results have been related to the stagnation line heating rates predicted by the $\varrho_T \mu_T$ and Cohen similiarity infinite cylinder theories calculated at the appropriate effective sweep angle:[11]

$$\sin \lambda_{eff} = \cos \beta \cdot \cos \alpha \cdot \sin \lambda - \sin \beta \cdot \cos \lambda \qquad (13)$$

The $\varrho_T \mu_T$-values lie consistently above the Cohen solution probably due to the applied $\varrho_T \mu_T$-correlation. The leading edge predictions fit the data well at $\alpha = 0^\circ$ and $\alpha = 45^\circ$ but overpredict the test results at $\alpha = 30^\circ$. This discrepancy may be declared by an increasing influence of the flat bottom on the blunt leading edge causing a more rapid stagnation line shift than predicted by eq. 12. This phenomenon has been discussed earlier by A.L. Nagel et al.[11]
At 45° angle of attack the stagnation line is finally shifted toward the bottom centreline and infinite cylinder solutions appear to underpredict leading edge heat transfer.
The interdependency between the flat bottom and the blunt leading edges may be studied to more extent from circumferential heating distributions. The figures 12 through 15 summarize the test data obtained at Cross-section 3,5 and 7. The normalized heating rates have been plotted over a spanwise surface coordinate which was related to the local width of a section normal to the leading edge.
Theoretical values were obtained from the infinite cylinder similiarity solution applied directly on the blunt leading edge or in a modification[9] on the crosswise flow starting at the bottom centreline with the circular disk - velocity gradient from ref. 10. In addition strip calculations with different pressure estimations are shown at 15 and 30 degree angle of attack.

Circumferential Heating Distribution Around Backward Body-Sections

α = 15°, β = 0°

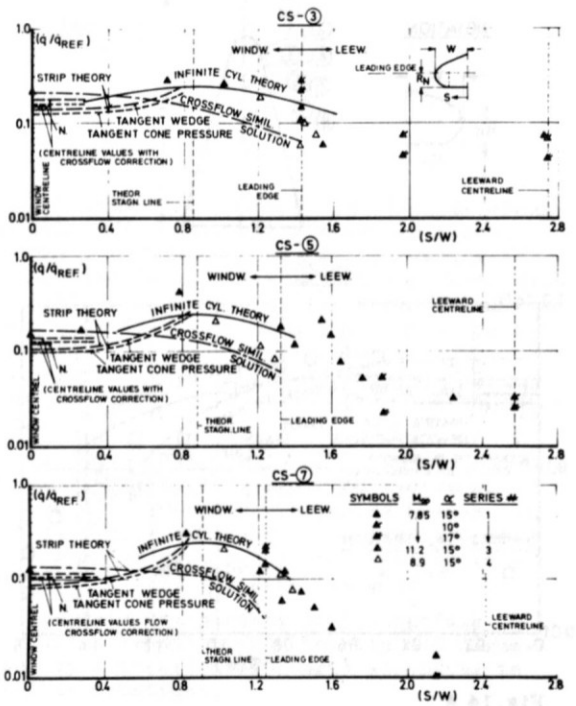

Fig. 13

The $\varrho_\tau \mu_\tau$ theory has been applied by simply assuming length coordinates on lines parallel to the centreline with the starting point at the stagnation line. On the centreline the increase of the strip flow value by application of the sharp delta wing crossflow correction is shown.

For zero angle of attack fig. 12 confirms the underprediction of stagnation line heating by the infinite swept cylinder theory. The difference diminishes toward the rear of the body which indicates nose bluntness effects. This is verified by the fact that the data off the centreline are well predicted by the infinite cylinder solution.

At α = 15° fig. 13 shows a considerably scatter of the test data. However, the stagnation line heating still appears to be underpredicted but no systematic decay of the difference may be observed.
The Tempilaq data taken at the higher Reynolds number in addition indicate a stronger flow expansion toward the outer edge than the Shock tunnel data. The strip flow and crossflow calculations both underestimate the heating level on the flat bottom in accordance to the streamline pattern shown in fig. 5. Nevertheless on the centreline the modified crossflow solution provides the best heating prediction.

An improved accuracy in heating predictions by the crossflow solution can only be expected at higher angles of attack when crosswise gradients start to predominate. Fig. 14 A shows this effect at thirty degree angle of attack for the forward section 3 where the flat portion is very small and the flow directly expands from the centreline.

Bottom Spanwise Heating Distribution

α = 30° ; β = 0°

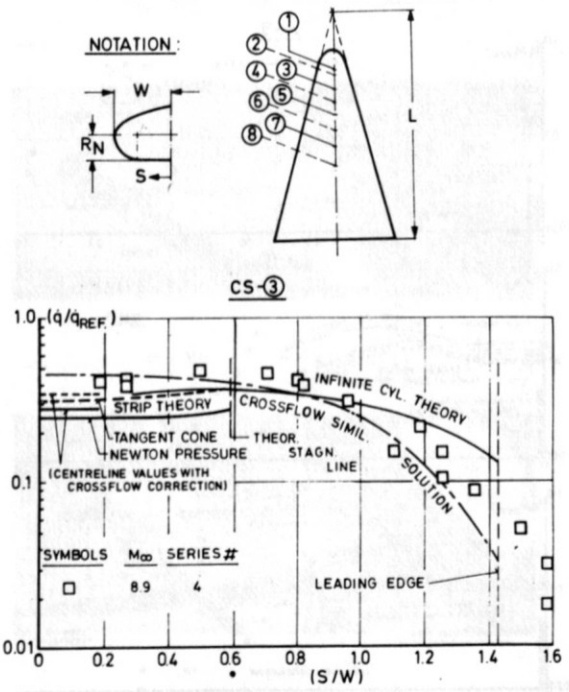

Fig. 14 A

Bottom Spanwise Heating - α = 30° - Continued

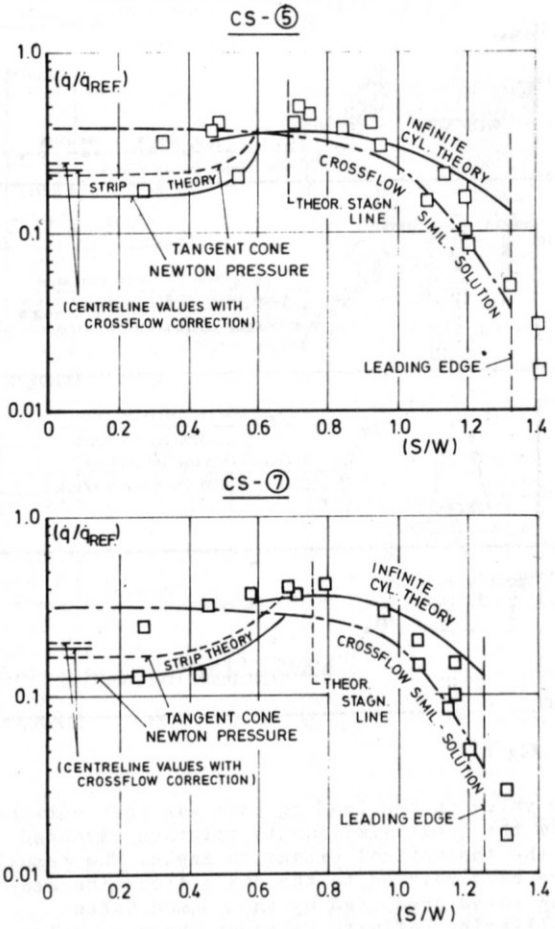

Fig. 14 B

However, due to the straight streamlines seen from the oil flow photograph the crossflow theory greatly overpredicts the bottom heat transfer at greater distances from the nose.

The stagnation line is believed to be still located on the cylindrical leading edge. For a proper prediction of the cylindrical heating distribution the stagnation line shifting due to the pressure adaption on the windward side must be taken into account.

Fig. 15 generally shows the same phenomenon for 45° inclination. It may be noted that the half shaded symbols in this plot indicate Tempilaq data taken at Mach 11.2 and 40° angle of attack.

The shock tunnel results are underestimated by the crossflow solutions off the centreline and the heating level on the slab portion seems only to become flat with growing distance from the apex. A maximum heating appears in the forward portion near the sonic point of the lateral velocity followed by an essential decay toward the leading edge.

Nevertheless, the Newtonian theory applied for the infinite cylinder calculation as well as for the crossflow expansion provides a stronger pressure decay than indicated by the heat transfer data.

The centreline heating rates obtained from strip flow calculations with oblique shock boundary layer edge conditions and sharp delta planform crossflow correction agree well with the similiarity stagnation point value (eq. 6) modified by a crossflow velocity gradient which accounts for edge bluntness.

This demonstrates that at large angles of attack leading edge effects do not exist any longer on the flat portion and the flow is processed through the local shock envelope.

Finally some data on the LB-21 centreline obtained from G. Koppenwallner and D. Vennemann[21] in the Low Density Nitrogen tunnel of AVA Göttingen may be shown. The measurements have been conducted at Mach numbers near 21 with a variation of Re_{∞}/ft from $4.8 \cdot 10^4$ to $1.1 \cdot 10^5$. This implies flow conditions above the continuum regime with $M_{\infty}/\sqrt{Re_{\infty}/ft}$-factors between $7 \cdot 10^{-2}$ and $1 \cdot 10^{-1}$.

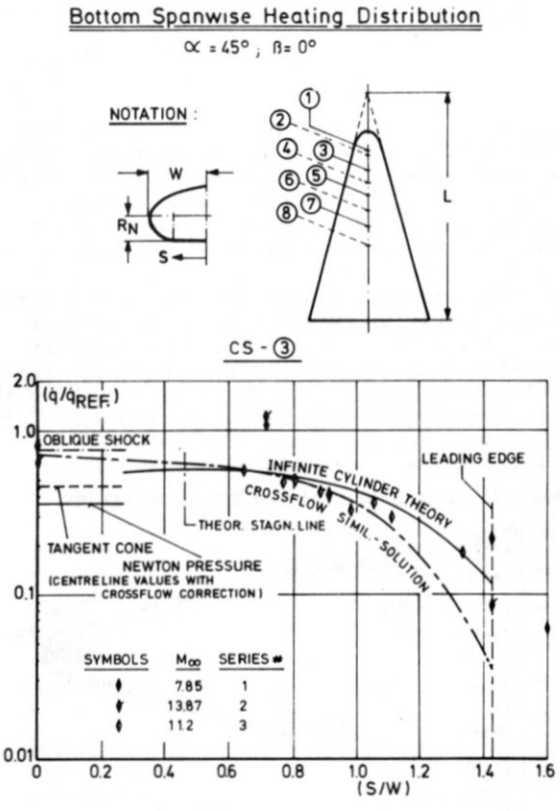

Fig. 15 A

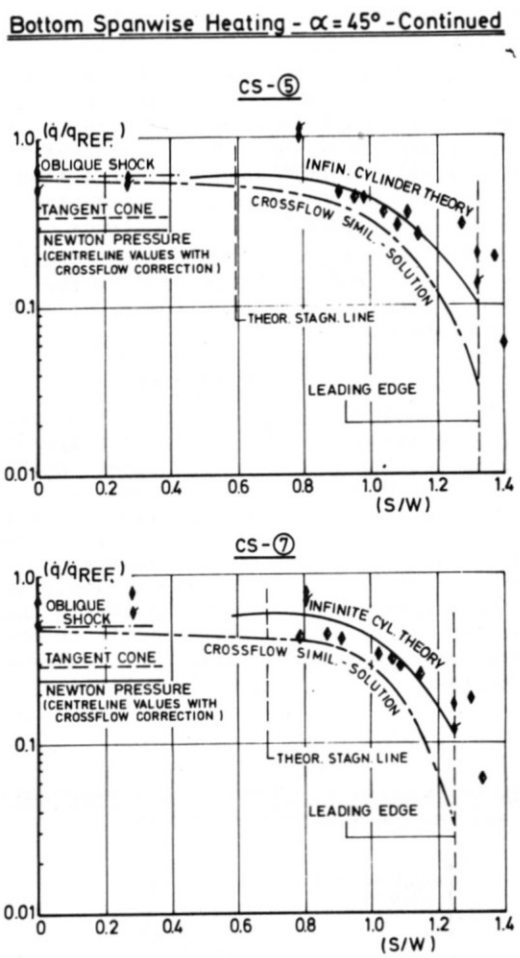

Fig. 15 B

Fig. 16 shows the heating distribution along the centreline over the stagnation pressure and Reynolds number range at zero angle of attack. The data indicate a strong decay from the nose to the aft end. The absolute heating level increases with stagnation pressure but the data fall essentially into one curve when normalized with the appropriate value from the gage 1 at the geometrical stagnation point.

In Fig. 17 the angle of attack dependency of centreline heating distribution is considered at a freestream Reynolds number per foot of $9.36 \cdot 10^4$. The local heat transfer is related at each run to the heating rate experienced from the nose tip gage.

The data are plotted over a surface coordinate measured from the tip and normalized by a theoretical length according to previous notations.

As might be seen from the figure the heating level is continuously increased with angle of attack.

In addition a decrease of the nose influence is indicated producing on almost linear decay at $\alpha = 35^{\circ}$. Reference measurements on a 0.3 in. sphere have shown a good agreement with L. Lees' theory[22] when the correction function of Ferry and Zakkay[23] accounting for vorticity interaction was applied.

Those interaction effects also appear to be of considerably influence over the forward portion of the lifting body at lower angles of attack.

Surface Temperatures

One of the main objectives of heat transfer studies is the definition of local temperature histories on the proposed configuration.[24] Thermal mapping tests are often used in development phases since they provide a quick survey on surface heating when reference values from calibration measurements are applied. However, problems arise in extrapolating those data to flight conditions according to the incomplete simulation capability. Therefore it had been proposed to evaluate the thermal environment for the full scale vehicle by

Bottom Centre Line Heat Transfer at Low Density Flow

ANGLE OF ATTACK-DEPENDENCY AT CONST. REYNOLDS-NUMBER

$M_{\infty} = 22.87$; $Re_{\infty}/ft = 9.36 \cdot 10^4$

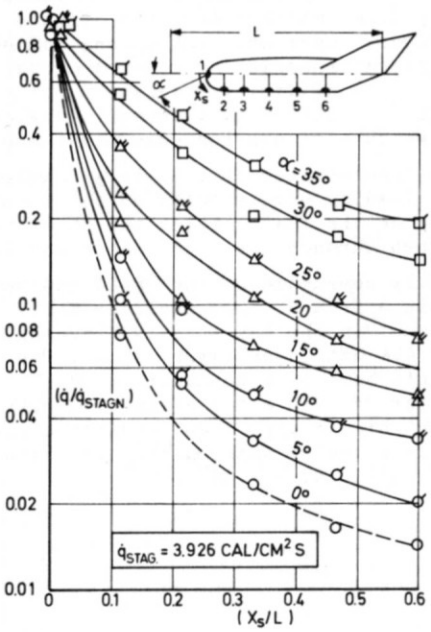

Fig. 17

Bottom Centreline Heat Transfer at Low Density Flow

INFLUENCE OF REYNOLDS-NUMBER AT ZERO INCLINATION

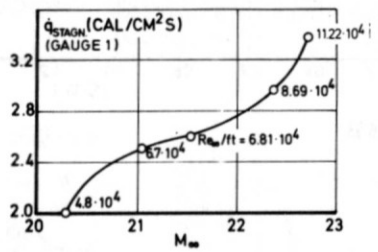

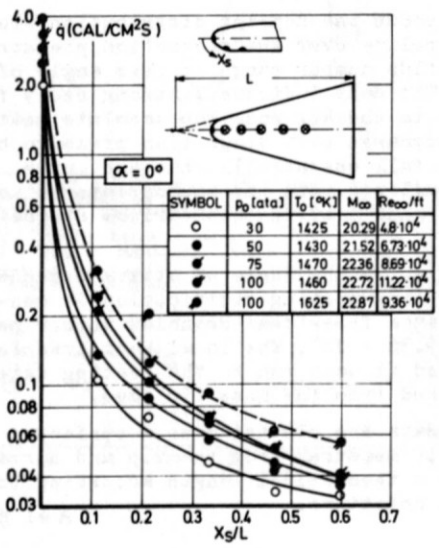

Fig. 16

application of the heat transfer coefficient ratio (h/h_{ref}) instead of the heating rates. The local adiabatic wall temperature at flight conditions may then be taken into account. This has not be done in the present study but a rude estimation will be shown for completeness.

Fig. 18 summarizes radiation equilibrium temperatures resulting from Thermocolor-tests at $M_{\infty} = 11,2$. The temperatures were directly evaluated from the experimental heating rates. Results according to 40° angle of attack on the lower surface are combined with zero angle of attack data for the upper side in order to show the highest possible temperatures.

Resulting Equilibrium Temperatures From Thermal Mapping Tests

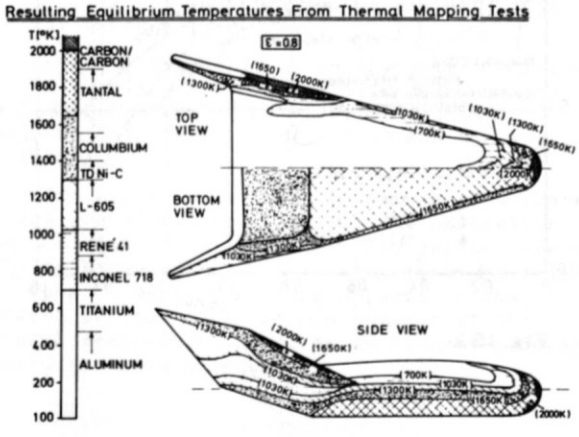

Fig. 18

Concluding Remarks

The foregoing study has illustrated some of the problems involved in the definition of thermal environment on delta planform reentry vehicles. The flow fields over these vehicles are three-dimensional and change considerably with angle of attack.
Different effects due to fuselage bluntness and shock interference must be taken into account. However, calculations have shown that realistic estimates of heating rates can be made by means of simplified assumptions provided three-dimensional effects are accounted for. In order to evaluate those influences heat transfer tests, pressure measurements and flowfield visualization techniques remain necessary until satisfactory analytical prediction methods for the inviscid flow field are available.
Thermal mapping tests have been shown to be an useful implement in heat transfer investigations even for quantitative analysis.

Summarizing we may say that on the proposed highly blunted lifting body configuration the flowfield on the windward side is essentially influenced by the blunt prow and the leading edge.Whereas bluntness effects on the flat bottom rapidly diminish with increasing angle of attack those effects remain in regions close to the leading edge at higher angles of attack.
Supplemental pressure measurements and flow field investigations would be helpful in interpreting those phenomena as well as in extrapolating test data to actual flight conditions.

References

1. Tolle, H. et al.,"Entwicklung der Konfiguration eines aerodynam. Wiedereintritts-Flugversuchskörpers unter besonderer Berücksichtigung der Stabilität und der Manövrierbarkeit"., Jahrbuch 1970 der DGLR, pp. 59-74.
2. Moore, F.K., Chapter on three-dimensional boundary layer theory in "Advances in Applied Mechanics", Vol. 4, 1956
3. Cooke, J.C., Hall, M.G., "Boundary Layer in three dimensions.", RAE-report, N°-Aero 2625, Febr. 1960.
4. Eichelbrenner, E.A., Oudart, A., "Méthode de calcul de la couche limite tridimensionelle"., ONERA, Pub.N° 76, 1955
5. Vaglio-Laurin, R., "Laminar Heat Transfer on three-dimensional blunt nosed bodies in hypersonic flow.", ARS Journal, vol-29, N° 2, Febr. 1959, pp. 123-129.
6. Beckwith, I.E., "Similiarity Solutions for small crossflows in laminar compressible boundary layers", NASA TR R-107, 1961
7. Stewartson, K."Correlated incompressible and compressible boundary layers", Proc. Roy. SOC. A, Vol. 200, p.84, 1949
8. Cohen, N.B., "Boundary layer similar Solutions and Correlation Equations for laminar heat transfer distribution in equilibrium Air at velocities up to 41100 Feet per second.", NASA TR R-118,1961
9. Beckwith, I.E., Cohen, N.B., "Application of similar solutions to calculation of laminar heat transfer on bodies with yaw and large pressure gradient in high-speed flow", NASA, TN D-625, 1961.
10. Bertram, M.H., Henderson, A., "Recent hypersonic studies of wings and bodies", ARS-Journal, Vol. 31, No. 8, Aug. 1961, pp. 1129-1139.
11. Nagel, A.L., Fitzsimmons, H.D., Doyle,L.B., "Analysis of hypersonic pressure and heat transfer tests on delta wings with laminar and turbulent boundary layers", NASA CR-535, 1966.
12. Fay, J.A., Riddell,F.R., "Theory of stagnation point heat transfer in dissociated Air", Journ. Aero. Sci., Vol. 25,No. 2, Febr. 1958.
13. Grönig, H. "Stosswellenrohre und Stosswellenkanäle"., 9. Raumfahrtlehrgang, März 1971, Band 1, Vortrag 04.
14. Heyser, A., Pfeiffer, H., Schepers, H. J., "Der Hyperschallwindkanal H_2 der DFVLR in Porz/Wahn", Jahrbuch 1969 des Landesamtes für Forschung in NRW., Seite 301-332.
15. Wuest, W., Koppenwallner, G., Hefer, G. Legge, H., "Der hypersonische Vakuum Kanal der Aerodyn. Versuchsanstalt Göttingen", Jahrbuch 1969 der DGLR, Seite 38 - 58.
16. Vidal, R.J., "Model instrumentation techniques for heat transfer and force Measurements in a hypersonic Shock tunnel", Cornell Aero. Lab., Rep. No. AD-917-A-1, Febr. 1956.
17. Carlslaw, H. S., Jaeger, J. C., "Conduction of heat in solids", Clarendon Press, Oxford, 1959.
18. Cérésuela, R., Bétrémieux, A., Cadars, J. "Mesure de l'échauffement cinetique dans les souffleries hypersoniques au moyen de peintures thermosensibles," ONERA, Pub. No. 313, 1965
19. Jones, R.A., Hunt, J.L. "Use of fusible temperature indicators for obtaining Quantitative Aerodynamic heat transfer Data", NASA TR R-230, Febr. 1966.
20. Schepers, H.J., Will, E. "Wärmeübergangsverhalten des Lifting-Body-Modells der Fa. ERNO, Bremen, bei der Anströmmachzahl 8.9", DFVLR-Bericht No. RV I1-05/14/70 März 1972.
21. Koppenwallner, G., Vennemann, D. "Wärmeübergangsmessungen an einem Modell des ERNO Lifting-Body LB-21", DFVLR-AVA-Bericht No. IB 063-72 H03, März 1972.

22. Lees, L., "Laminar heat transfer over blunt nosed bodies at hypersonic flight speeds", Jet Prop., Vo. 26, No. 4, 1956, pp. 259 - 269.

23. Ferri, A., Zakkay, V., "Blunt body heat transfer at hypersonic speed and low Reynolds numbers", Journ. Aero.Sci., Vol. 28, No. 12, 1961, pp. 962-971.

24. Zimni, W.F., Hoffmann, J.P., Rätz, E.A. "Die thermische Belastung eines aerodynam. Wiedereintrittskörpers und die daraus resultierenden Optimierungs- und Auslegungskriterien", Raumfahrtforschung, Heft 2, März/April 1970.